NOTES AND CORRESPONDENCE

Near-Surface Current Measurements Using a Ship-Deployed ''Horizontal'' ADCP

GEORGE O. MARMORINO AND CLIFFORD L. TRUMP

Remote Sensing Division, Naval Research Laboratory, Washington, D.C.

ZACHARIAH R. HALLOCK

Oceanography Division, Naval Research Laboratory, Stennis Space Center, Mississippi

5 November 1998 and 8 April 1999

ABSTRACT

An experiment was performed to measure the near-surface current by aiming horizontally two of the beams from an acoustic Doppler current profiler (ADCP) deployed at 0.6-m depth from an anchored (but rolling) ship. The results compare favorably with independent current measurements made at 2-m depth but appear to resolve as well a vertical current shear associated with the shallow wind-drift layer. The approach, therefore, has potential for investigating the current profile in the upper meter or two of the water column.

1. Introduction

There continues to be considerable interest in the current profile close to the sea surface where the effects of wind stress, wind waves, and buoyancy flux are important and where practical application to such problems as the advection of surface pollutants, search and rescue operations, and air–sea exchange of momentum and mass has led to various schemes to measure and parameterize the near-surface flow (e.g., Csanady 1997). Recent studies demonstrate how radar-based techniques can probe the upper meter or so of the water column, offering uniquely detailed views of the current structure and providing intriguing new insights (e.g., Fernandez et al. 1996; Moller et al. 1998). As the interpretation of such measurements involves assumptions about the vertically integrated effects of the current profile on the surface waves, it is important they be validated using independent measurements. Thus it is of interest to consider how existing, in situ, current-measuring technology might be better applied to this problem.

In this note we report an attempt at measuring the near-surface current using a common type of acoustic Doppler current profiler (ADCP) having narrow ''pencil'' beams. The measurements were made by rigidly mounting the ADCP off one side of an anchored research vessel but orienting it horizontally (instead of vertically downward, as is usually done) so that two acoustic beams are aimed sideways, away from the ship. Because the ADCP is deployed close to the sea surface, the acoustic return for a near-horizontal beam will be dominated (under at least moderate winds) by backscatter from a nearly continuous layer of small air bubbles generated by the intermittent breaking of surface gravity waves (e.g., Thorpe 1986; Crawford and Farmer 1987). However, because of the rolling motion of the ship, the beam angle made with the horizontal is constantly changing, so attention must be paid to the roll angle associated with each acoustic ping. Measurements made using ''fan-shaped'' beams (broad in elevation and narrow in azimuth) avoid this angle sensitivity (e.g., Smith 1998; Plueddemann et al. 1999) but at the expense of vertical resolution. A question is whether the varying roll angle and narrow beams can be exploited in our case to provide quasi-vertical current profiles.

The measurements were made during the third Chesapeake Bay Outflow Plume Experiment (COPE-3), which was conducted from early October through November 1997. As part of this field program, six bottom-mounted, upward-looking ADCPs were deployed across the inner shelf south of the bay mouth (Vesecky et al. 1998). The horizontal-looking ADCP measurements reported in this paper were made during 8–10 October (days 281–283), under low to moderate wind and sea conditions, while the ship was anchored near an ADCP

Corresponding author address: George O. Marmorino, Remote Sensing Division, Code 7250, Naval Research Laboratory, Washington, DC 20375-5351.
E-mail: marmorino@nrl.navy.mil

mooring. This allows a comparison to be made between the two types of ADCP measurements. The results reported here, while of a limited and preliminary nature, might serve to encourage additional studies of this kind.

2. Approach

a. Instrumentation

The horizontal measurements were made using a 307-kHz narrowband ADCP manufactured by RD Instruments. The ADCP was deployed by clamping it to a vertical support pole located on the port side of the R/V *Cape Henlopen,* about 3.5 m off the ship's centerline. (The pole is typically used to mount a downward-looking 1200-kHz ADCP for underway measurements.) The transducer was oriented so that two beams were approximately horizontal—one pointing 30° forward, the other 30° aft. To prevent interference with these horizontal beams, the two remaining beams (lying in the vertical plane) were suppressed by covering the transducers with a sound-absorbing material. The mean depth of the transducer was 0.6 m. Depth variations induced by the roll of the ship (e.g., a 10% depth change for a 1° roll) are ignored in the analysis. Previous studies (e.g., Crawford and Farmer 1987) show that the mean bubble distribution has a vertical scale depth of about 1 m for winds less than about 10 m s^{-1} (the case here); thus, the transducer was, on average, located well within the bubble layer. Two orthogonally positioned angle sensors were mounted above the ADCP to measure pitch and roll. While the resolution of these measurements ($\approx$0.2°) was adequate, absolute values (especially of the roll sensor) are uncertain because of unmeasured offsets in mounting the sensor assembly. An additional uncertainty is the true pointing direction (azimuth) of the beams as only an approximate alignment was made between the midbeam centerline mark on the pole and the side of the ship. This azimuth uncertainty is estimated as being less than 10°.

Data from each acoustic ping were recorded (100 pings per minute) using the manufacturer's data-acquisition program TRANSECT. The ''bin'' or range cell size was set at 1.18 m (the minimum allowable value) and 120 bins of data were collected from each beam. Data from the pitch and roll sensors were recorded directly into the ADCP data stream so that values could be assigned to each ping. The first bin was centered at a range of 4.15 m from the transducer and the last bin was thus at a range of 144.6 m. (Data from the first few bins often appeared spurious, possibly the result of sidelobe effects, and were generally ignored in the analysis.) Data were averaged over time to reduce single-ping noise (about 30 cm s^{-1} rms), to provide sufficient numbers of data points over a range of roll angles, and to reduce the effect of surface-wave orbital velocity. Each acoustic beam has a 3-dB width of 2.2°. Using this value and the mean depth of the transducer, a horizontal beam will spread vertically to first intersect the surface at a range of about 32 m. The variable beamwidth plus the nonuniform vertical weighting of the returns induced by the bubble distribution may be expected to result in an effective measurement depth that varies in range even for a ''horizontal'' beam.

The ADCP mooring measurements were made using 300-kHz broadband instruments deployed on the bottom in trawl-resistant housings. Six moorings were deployed on 5 October. Following deployment (6–7 October), measurements of surface hydrography and currents were made across the mooring array. Five of the moorings were recovered on 10 November; data from A1 and A4 will be used for comparisons with the horizontal measurements. The sampling scheme was a 1-min burst of 120 samples every 5 min. Burst sampling was used to minimize aliasing by surface gravity waves. The vertical bin size was 1 m and data were collected starting from about 3 m from the bottom. The shallowest valid current data were judged to be from the bin located 2 m below the mean sea surface. Returns from shallower bins generally had vector directions closely aligned with the wind vector but maximum speeds of about 1 m s^{-1} for moderate wind speeds. This result is consistent with previous ''surface velocity'' measurements made by Schott (1989) and Narajima et al. (1995) but appears to disagree with much lower surface speeds measured by Zedel et al. (1996). As the proper interpretation of the near-surface Doppler returns in our dataset is unclear, their analysis is not pursued in this paper.

b. Anchor stations

To allow time averaging and data comparisons, the ship was anchored near an ADCP mooring. Bow and stern anchors were used to minimize heading fluctuations. Anchoring also allowed turning off the main engine and its coolant water, which normally would discharge just forward of the ADCP pole. The hydraulic coolant discharge (located just astern of the pole) was also turned off. These two discharges normally make large, continuous clouds of bubbles. Two remaining and lesser discharges (from a generator and a water maker) located astern of the pole remained on but minimally disturbed the water. To explore the effects of the two major discharges, data were collected with the discharges cycled on and off for test periods of 10-min duration. These showed that acoustic backscatter levels were lower with the discharges on (likely because of signal loss through the discharge-generated bubble clouds) but that there was no discernible degradation of the radial velocity data.

Measurements were made at both inshore and offshore anchor stations (Fig. 1). The inshore station (36°51.771′N, 75°56.651′W; water depth of about 10 m) was located 0.50 km from ADCP mooring A1 (36°51.85′N, 75°56.3′W). The offshore station (36°52.85′N, 75°47.52′W) was centered among four of

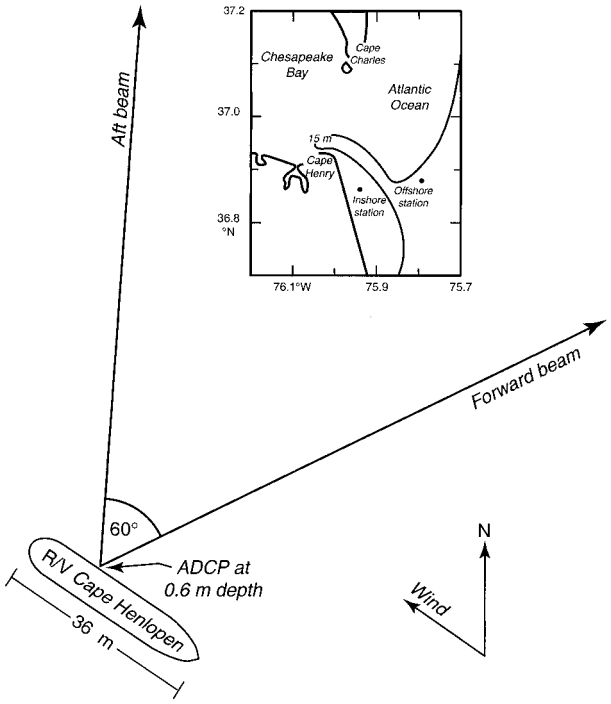

FIG. 1. Experiment arrangement at the inshore station. (Inset shows location of both inshore and offshore stations.)

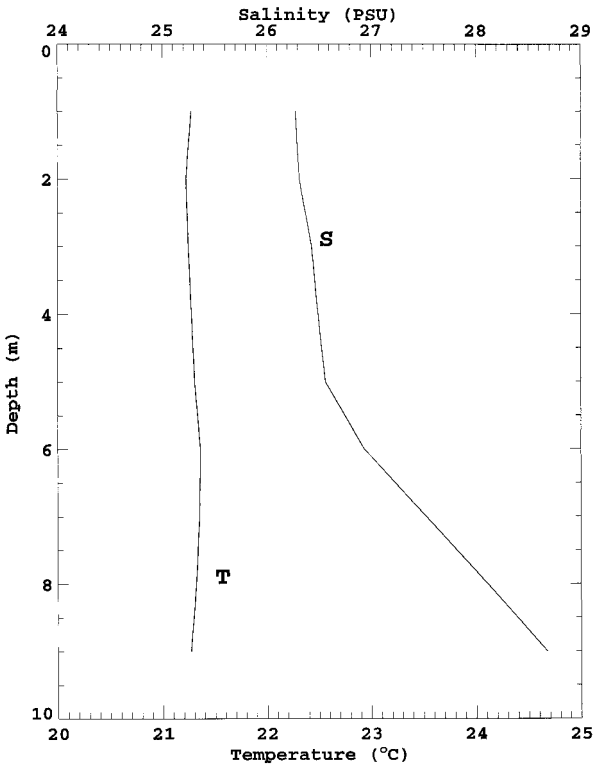

FIG. 2. Temperature and salinity profiles made at mooring A1 on 7 Oct to illustrate conditions inshore.

the ADCP moorings (A3–A6). All but mooring A6 were later recovered. Data from the offshore station are compared with mooring A4 (36°52.00′N, 75°46.90′W), which was located 1.81 km from the ship and in similar water depth of about 18 m. Although the ship was anchored, periods of gusty winds produced horizontal swaying motion with a period of about 5 min and an amplitude as large as 5 cm s^{-1}. (The ship's motion was determined from DGPS measurements.)

Figure 1 shows the configuration at the inshore station. Measurements were made from 1535 LT 8 October to 0310 LT 9 October, nearly one M_2 tidal period in length. The mean wind speed (measured at mast height) was 5.0 m s^{-1}. The mean wind direction was 123°T, but there was a gradual 70° clockwise rotation of the wind over the period. The ship's heading was southeastward (mean of 124°) and thus approximately into the wind. Seas were 0.3 m high and there was a low-amplitude, 50-m wavelength swell from the southeast. (The swell thus approximated a shallow-water wave at the inshore station.) Hydrographic measurements at mooring A1 (Fig. 2) show that the inshore water was vertically stratified due to a shallow layer of low-salinity ($S \approx 26.5$ psu) plume water overlying higher-salinity shelf water; temperature stratification was negligible. Based on the salinity variation alone, the sound speed increased with depth by about 3 m s^{-1}. This increase resulted in a gradual upward refraction of initially down-going acoustic beams. When large vertical current shear was present in the water column, refraction-induced ''turning points'' appeared in plots of the measured radial velocity versus range (for a given roll angle). For example, beams aimed downward at 1°, 2°, and 3° showed turning points in the data at increasing ranges of 100–120 m, behavior that was consistent with ray-tracing calculations.

Measurements were made at the offshore station from 0915 LT 9 October to 1000 LT 10 October. We will examine an 11.5-h subset covering the periods 1600–2230 and 0530–1030 LT. The gap corresponds to a period when the outflow plume passed through the measurement domain, resulting in horizontally variable conditions. As the plume passed the offshore station (at 2342 LT), the surface salinity dropped 1.5 to about 29 psu. Compared with the inshore station, salinity stratification was weaker and temperature stratification no longer negligible. Over the subset period, the mean wind was 6.7 m s^{-1} from 190°T, but again there was significant rotation over time. The mean ship's heading was in this case southwestward (208°T).

3. Processing

a. Selection of horizontal pings

Because of uncertainty in the absolute measurement of roll angle, we needed a means to determine the roll angle corresponding to a horizontal ping. The scheme used for this is based on a plot of roll angle θ versus

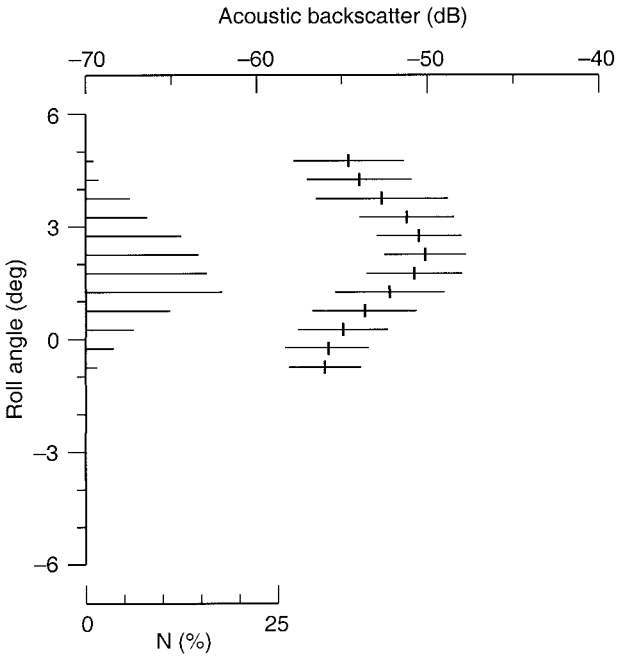

FIG. 3. Variation of the mean acoustic backscatter intensity with roll angle. Data are from the aft beam averaged over 1 h (0020–0120 LT 8–9 Oct) and over range bins 40–90. Backscatter (units of relative intensity in dB) has been corrected for signal attenuation and absorption. Error bars show the standard deviation about the mean. Horizontal lines extending from the roll axis show the number N of data values in each 0.5° roll-angle interval.

acoustic backscatter intensity, such as shown in Fig. 3 for the aft beam. The plot shows a well-defined backscatter peak occurring at a roll angle $\theta_{max} \approx 2.5°$. While the figure shows results averaged over the midrange (bins 40–90), the range dependence of θ_{max} was also investigated and found to be generally less than 1°, that is, less than the acoustic beamwidth. We assume the backscatter peak arises from beam trajectories through the bubble layer. As the thickness of the bubble layer is comparable to the transducer's depth, these trajectories are nearly horizontal; therefore, $\theta = \theta_{max}$ is the approximately horizontal roll angle. Relative downward-going beams ($\theta < \theta_{max}$) thus show lower backscatter values because the returns are from the ambient water column, which contains mostly low-intensity scattering targets of biological origin; up-looking beams ($\theta > \theta_{max}$) also show lower values because these beams reflect downward from the surface and so also sample the low water column values. Similar values of θ_{max} were found for the aft beam at both the inshore and offshore stations except during a calm period (excluded from the analysis presented later). At these low wind speeds (≤ 3 m s^{-1}), the backscatter peak occurred at a more upward roll angle. This would be consistent with the bubble layer being shallower than the transducer in this case, or with a scattering contribution from acoustically resonant capillary waves.

Behavior similar to that in Fig. 3 was found for the forward beam except that the backscatter peak occurred $\theta_{max} \approx 0°$. The different θ_{max} values resulted from an inadvertent mean tilt of the transducer housing, which was measured to be about 3° bow-upward. The forward beam was thus biased upward, and the majority of its data points corresponded to relative upward roll angles ($\theta > \theta_{max}$). On the other hand, the distribution of data points for the aft beam is peaked near its θ_{max} value (Fig. 3, left), indicating that the bulk of the aft-beam data is for a horizontal look. For this reason, examination of the aft beam has been generally more informative.

b. Systematic measurement bias

For a near-horizontal (or near-grazing angle) beam, a potential problem is shadowing by troughs of the swell (Smith 1998). In such a case, the acoustic beams undersample the velocity under the crests and so the orbital wave velocity does not average out, resulting in an averaged radial velocity that is systematically biased either positively or negatively, depending on the beam direction relative to the swell propagation direction. Selected data subsets were examined to see if this effect is significant. A typical result is shown in Fig. 4, which shows the radial velocity plotted against range for 50 consecutive acoustic pings (30 s of data). The roll angle for each ping is shown on the right of the figure. As the ship motion could not be removed on individual pings, the curves show only the signal relative to the range-averaged radial velocity on each ping. The swell signal appears in the plot as approximate sinusoids having an along-beam wavelength of about 70 m and an amplitude of about 25 cm s^{-1}. (In the case shown, the beam direction was approximately eastward and the swell direction from the southeast.) The approaching swell appears as patterns of closely bunched curves moving toward the transducer over time. Overall, the swell crests and troughs appear about equally well in the figure, at near range and far; hence, shadowing does not appear to be a severe problem in our dataset.

Also note in Fig. 4 that the roll is generally more random and shorter in period than the swell. Thus the roll of the ship does not vary coherently with the swell. The result is that under such conditions a time average (for a particular roll) will not be biased toward a particular phase of the swell. It is expected that this result will in general be sensitive to the interplay between the ship-mooring dynamics and the environmental conditions.

c. Computation of vector current

To compute a vector surface current, range-averaged radial velocities from horizontal pings from both beams were combined. Combining the data in this way assumes the spatial scale of the flow is large compared with the separation between the two beams, which is of the order of 50 m (e.g., Fig. 1). This is a reasonable assumption

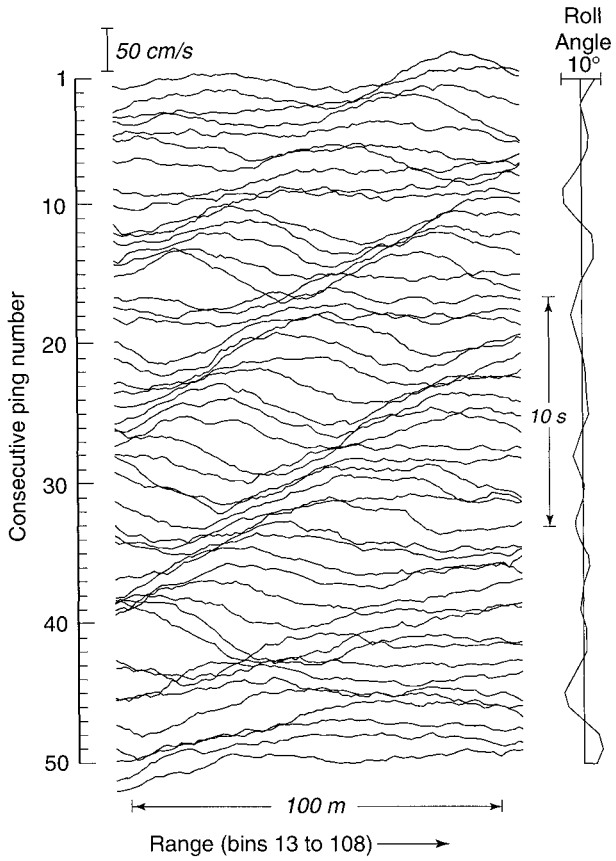

FIG. 4. Radial velocity vs range shown for 50 consecutive acoustic pings, beginning at 0053:30 LT on day 283. The data have been smoothed in range (25-m running average) to reduce noise. The range direction in this example is 083°T.

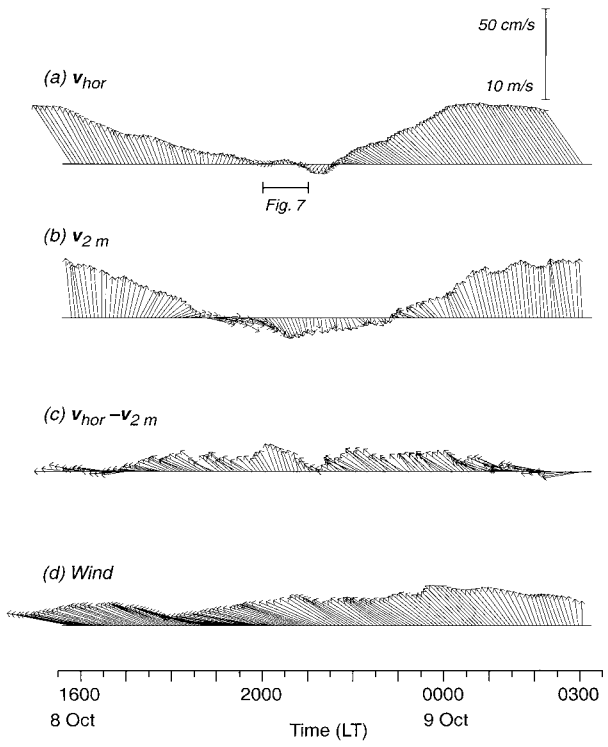

FIG. 5. Time series of current vectors derived from (a) horizontal ADCP measurements; (b) ADCP mooring A1 measurements; (c) the vector difference, $\mathbf{v}_{hor} - \mathbf{v}_{2\,m}$; and (d) the shipboard vector wind. The horizontally derived vectors use data constrained to be within 1° of horizontal (i.e., roll-angle interval of $\theta_{max} \pm 1°$). The data sample interval is 5 min for each variable; data have been smoothed over five consecutive intervals.

for homogeneous conditions (i.e., away from fronts) and for suitable averaging periods. An averaging period of 5 min was chosen to match that of the moored ADCP measurements. Horizontal pings are taken as those having roll angles satisfying $|(\theta - \theta_{max})| \leq 1°$, that is, a 2° interval comparable to the width of the beams. The sensitivity of the results to this choice is examined below. To reduce noise, the data were averaged over range bins 40–90. This subset of bins had the least variation in θ_{max} in each beam. Also, elimination of the near range avoids data contaminated by ship-induced flow disturbances, as inevitable directional changes in the current and wind caused some of the range bins to lie in the lee of the ship. Finally, to provide absolute (earth-referenced) currents, the horizontal currents were corrected for the average horizontal ship motion in each 5-min period.

4. Results

a. Vector current comparisons

Time series of the vector surface current $\mathbf{v}_{hor}$, computed from the horizontal measurements as described above, are shown in Fig. 5 for the inshore station and in Fig. 6 for the offshore station. Also shown in the figures is the 2-m depth current, $\mathbf{v}_{2\,m}$, measured at moorings A1 and A4. At the inshore station (Fig. 5), currents at the beginning and end of the record are relatively strong in both sets of measurements, but the mooring-measured flow is directed northward, while the horizontally measured flow is northwestward and better aligned with the vector winds (shown at the bottom of the figure). The flow is weaker over the middle of the time series, as the tidal current has rotated to oppose the wind-driven flow. It is during this period that differences between the two sets of measurements become clearest. For example, at 2030 LT, the 2-m depth flow is southward at about 10 cm s^{-1}, while the horizontally measured flow is weakly northward. At the offshore station (Fig. 6), the tidal currents are weaker (about 13 cm s^{-1} amplitude) so that the near-surface currents are dominated by the wind. Time series of the vector difference $\mathbf{v}_{hor} - \mathbf{v}_{2\,m}$ are shown in the third panel of Figs. 5 and 6. At both stations, the difference vector has a magnitude of about 10 cm s^{-1} and tends to be aligned approximately with the wind vector. This suggests the difference arises from vertical shear induced by the wind.

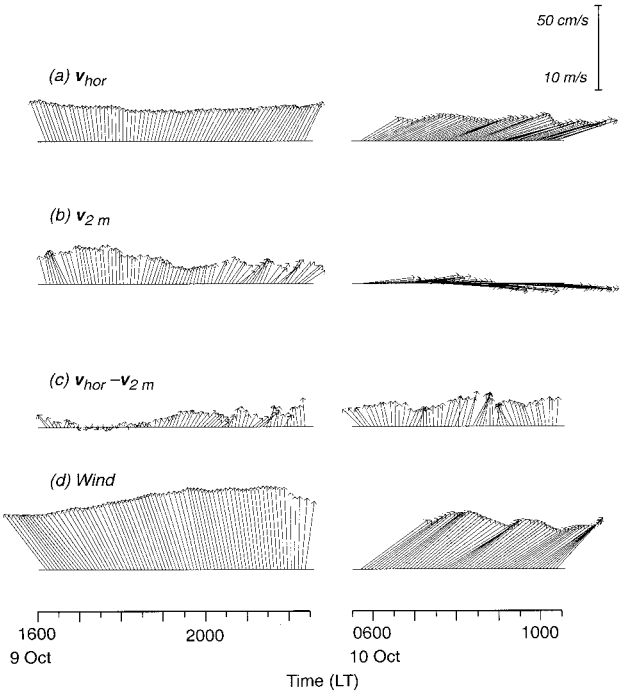

FIG. 6. As in Fig. 5 but for the offshore station and ADCP mooring A4.

To quantify the relationships between the various vector time series, a (complex) vector correlation coefficient was computed (Kundu 1976). The magnitude of the correlation coefficient provides an overall measure of correlation between the vectors; and its phase angle gives the average counterclockwise angle of the second vector with respect to the first, where the averaging is weighted by the magnitude of the instantaneous vectors. We also computed the complex transfer coefficient (Noble et al. 1996), the magnitude of which gives the amplitude of response (or gain) between two vector series. All these results are summarized in Table 1. At the inshore station, the correlation coefficients are reasonably high except between the wind and the 2-m current, which is more affected by the strong tidal variability. At both stations there is a clockwise rotation between the wind and $\mathbf{v}_{hor}$ (by 16°–18°) and between $\mathbf{v}_{hor}$ and $\mathbf{v}_{2\,m}$ (11°–27°), which is consistent with Ekman dynamics. These directional differences are significant when compared to the azimuthal measurement uncertainty ($\leq$10°). Confidence limits on the phase angles were derived from numerical simulations using both artificial data and subsets of the actual observations; these showed that for a vector correlation coefficient of 0.85 the expected error in phase angle was of the order of 1°. Notice that at the offshore station, the phase angles add consistently (i.e., $-11° + -16° = -27° \approx -26°$) as the correlations are high; this is not true at the inshore station because the wind–$\mathbf{v}_{2\,m}$ correlation is so low (0.31).

The gain between the wind and horizontally measured current is about 0.03 for both stations. This is consistent with previous results that show the wind-drift velocity to be about 3% of the wind speed (e.g., Csanady 1997). The gain between the wind and 2-m current is less (about 1%–2%), indicating a weaker response to the wind forcing; similarly, the magnitude of the 2-m current is only about 70% of the horizontally measured current. Also, the mean angular difference between the wind and difference vectors is small (4°–11°), indicating that the wind and vertical shear are approximately aligned. These results suggest the horizontal measurements include a response to the shallow wind-drift layer and, hence, provide more realistic surface currents than the measurements made at 2-m depth.

TABLE 1. Summary of complex correlation and transfer coefficients. A negative phase angle indicates vector 2 is rotated clockwise looking downward from vector 1.

Vector 1	Vector 2	Gain	Correlation	Phase angle
Inshore station				
$\mathbf{v}_{hor}$	$\mathbf{v}_{2m}$	0.69	0.85	−27°
Wind	$\mathbf{v}_{hor}$	0.027	0.64	−18°
Wind	$\mathbf{v}_{2m}$	0.011	0.31	−63°
Wind	$\mathbf{v}_{hor} - \mathbf{v}_{2m}$	0.021	0.75	4°
Offshore station				
$\mathbf{v}_{hor}$	$\mathbf{v}_{2m}$	0.73	0.88	−11°
Wind	$\mathbf{v}_{hor}$	0.032	0.94	−16°
Wind	$\mathbf{v}_{2m}$	0.024	0.83	−26°
Wind	$\mathbf{v}_{hor} - \mathbf{v}_{2m}$	0.010	0.58	11°

b. Range and depth variation of radial current

In this section we focus on the period 2000–2100 LT (Fig. 5), which shows the horizontally measured flow being weakly northward, while the 2-m depth current is more strongly southward. To explore the source of this difference, we have recalculated the current by dividing the original 2° roll-angle interval into two 1° subintervals. These results are plotted against range in Fig. 7a. (Only results from the aft-looking beam are shown as this beam was aligned at 1.5°T and hence contains nearly all the significant flow.) The upper 1° subinterval (the solid curve in Fig. 7a) shows a weak northward flow, decreasing from about 4.5 cm s^{-1} (near range) to 2.5 cm s^{-1} (far range). The lower 1° subinterval (dashed curve) shows a similar weak northward flow in the near range, but at far range the flow is southward (like the 2-m depth flow measured at the mooring). This behavior suggests the near-range measurements from either subinterval are resolving the flow at relatively shallow depths (comparable to the 0.6-m transducer depth). However, because there is vertical spread of the beams with increasing range, the lower 1° measurements have an increasing contribution from deeper flow. Thus, we interpret the range dependency of the lower 1° subinterval as being due essentially to vertical current shear. At a range of 100 m or more the two 1° subintervals differ in current by about 5 cm s^{-1} (Fig. 7), while the

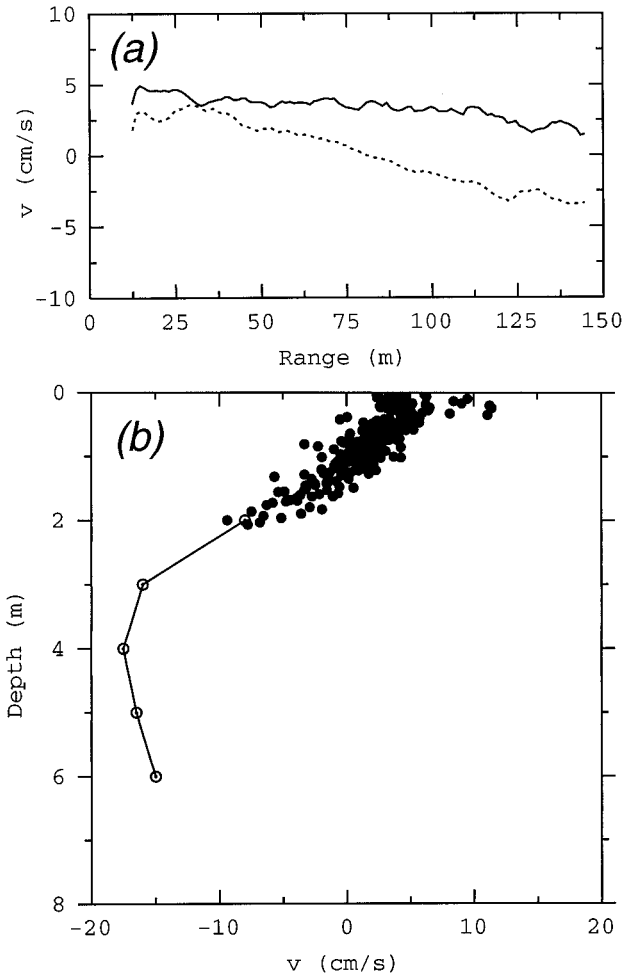

FIG. 7. (a) Range and (b) depth profiles of aft-beam radial velocity for 2000–2100 LT. The two curves in (a) show the range dependence of the horizontal current for the upper (solid) and lower (dashed) 1° subintervals of the original roll-angle interval used to compute the vector current of Fig. 5. The data points in (b) derive from near-range measurements (bins < 40) made over angles ranging from "horizontal" (i.e., $\theta = \theta_{max} \pm 0.5°$) to 1.65° downward. Beam refraction effects, judged to be relatively small in the near range, have been ignored in determining the measurement depths. Also shown in (b) is the mooring current component in the direction of the aft beam. Each of these measurements represents a vertical average over about 1 m.

(geometrical) vertical offset between them is 1.75 m. This gives a northward vertical shear $\partial v/\partial z$ of 5 cm s^{-1} divided by 1.75 m, or about 0.03 s^{-1}. This is, however, a lower bound because of vertical weighting of the returns by the bubble distribution.

Additional evidence of vertical shear is provided by examining the near-range measurements (bins < 40) from all the available pings, covering a roll-angle range from "horizontal" (i.e., $\theta = \theta_{max} \pm 0.5°$) to 1.65° downward in this example. These data points are plotted versus depth in Fig. 7b. While there is considerable scatter, the data show an approximately linear current profile extending from about 2-m depth to very near the surface. The northward vertical shear $\partial v/\partial z$ is now about 20 cm s^{-1} over 2 m, or about 0.1 s^{-1}, which is indeed larger than that estimated from Fig. 7a. For comparison, Fig. 7b also shows the corresponding current profile from mooring A1. Notice how northward shear between 3- and 2-m depth in the mooring profile seamlessly connects the mooring and horizontally measured profiles. While not all cases examined are as clear as this one, such comparisons do suggest the horizontal measurements can yield a realistic near-surface current profile.

5. Summary and discussion

We have reported on a set of shipboard measurements made using an off-the-shelf acoustic Doppler current profiler (ADCP) oriented so two of its beams were aimed approximately horizontally. Our purpose was to explore the potential of such an approach for measuring the current near to the sea surface where wind momentum is transferred to the water column but where the complicating effects of surface waves and bubbles normally make such measurements difficult. There were two principal objectives. The first was to demonstrate that such an approach might make precise current measurements close to the surface. The second was to explore whether one might make use of the rolling motion of the ship and the narrow width of the acoustic beams to achieve some profiling of the water column near the surface. These objectives were accomplished primarily through comparisons with currents measured by nearby bottom-mounted ADCPs.

The analysis shows that the horizontally measured currents compare favorably with measurements at 2-m depth from the moorings but show a greater response to the local wind. This is consistent with the shallow (0.6 m) depth of the shipboard transducer, which, except for low wind speed, was effectively embedded within the bubble layer and thus provided a shallow sampling depth for the horizontal beams. The mean horizontally measured current is about 3% of the wind speed, which is the expected level of response. Further examination of the range and depth dependence of the shipboard measurements suggests they resolve the vertical profile over the upper meter or two of the water column. Vertical shear associated with the wind-drift layer is expected to be concentrated in the upper meter (Csanady 1997). Therefore, it may be concluded that the measurements have resolved the vertical current shear associated with the shallow wind-drift layer. These preliminary results suggest the approach shows some promise for investigating the current structure near the surface and thus may serve, for example, as a useful adjunct to field experiments using multifrequency HF radars, which also measure the current in the near-surface region of 0.5- to 2.0-m depth, depending on the frequency of the instrument. These HF systems have become more common in coastal oceanography in recent years, but

the precise depth at which they measure the current is still an open question.

It would be of interest to make additional measurements after correcting certain defects in the technique. Improvements would include, for example, measurement of absolute roll angle. (We used the occurrence of a mean backscatter maximum to identify when a beam was horizontal.) Also, the shallow transducer depth and rigid mounting we used resulted in a large fraction of the data points having ambiguous interpretation as they derived from up-going beams (geometrically) intersecting the surface. These data points were ignored in the present study; however, simulation of the acoustic ray paths, taking into account reflection and scattering from a realistic rough sea surface, might lead to an understanding of how to exploit such data. Alternatively, other deployment configurations might be considered to improve the sampling. Also, while we have emphasized the measurement of time-averaged absolute currents in this report, ''horizontal'' ADCP measurements made while under way may be used to study transient horizontal flows such as those associated with ship wakes and propagating estuarine fronts (Marmorino and Trump 1996a,b; Trump et al. 1999).

Acknowledgments. This is a contribution to the Physics of Coastal Remote Sensing Accelerated Research Initiative, funded by the Office of Naval Research and managed at the Naval Research Laboratory by Dr. Richard Mied.

REFERENCES

Crawford, G. B., and D. M. Farmer, 1987: On the spatial distribution of ocean bubbles. *J. Geophys. Res.,* **92,** 8231–8243.

Csanady, G. T., 1997: The ''slip law'' of the free surface. *J. Oceanogr.,* **53,** 67–80.

Fernandez, D. M., J. F. Vesecky, and C. C. Teague, 1996: Measurements of upper ocean surface current shear with high-frequency radar. *J. Geophys. Res.,* **101,** 28 615–28 625.

Kundu, P. K., 1976: Ekman veering observed near the ocean bottom. *J. Phys. Oceanogr.,* **6,** 238–242.

Marmorino, G. O., and C. L. Trump, 1996a: Preliminary measurement of a ship's wake with side-scan ADCP. *J. Atmos. Oceanic Technol.,* **13,** 507–513.

——, and ——, 1996b: High-resolution measurements made across a tidal intrusion front. *J. Geophys. Res.,* **101,** 25 661–25 674.

Moller, D., S. J. Frasier, D. L. Porter, and R. E. McIntosh, 1998: Radar-derived interferometric suface currents and their relationship to subsurface current structure. *J. Geophys. Res.,* **103,** 12 839–12 852.

Nakajima, H., A. Kaneko, and N. Gohda, 1995: Sea surface measurement by a self-contained upward-looking ADCP. *J. Meteor. Soc. Japan,* **73,** 639–643.

Noble, M. A., W. W. Schroeder, W. J. Wiseman, H. F. Ryan, and G. Gelfenbaum, 1996: Subtidal circulation patterns in a shallow, highly stratified estuary: Mobile Bay, Alabama. *J. Geophys. Res.,* **101,** 25 689–25 703.

Plueddemann, A. J., E. A. Terray, and R. Merewether, 1999: Design and performance of a self-contained, fan-beam ADCP. *Proc. IEEE Sixth Working Conf. on Current Measurement,* San Diego, CA, IEEE, 54–59.

Schott, F., 1989: Measuring winds from underneath the ocean surface by upward-looking acoustic Doppler current profilers. *J. Geophys. Res.,* **94,** 8313–8321.

Smith, J. A., 1998: Evolution of Langmuir circulation. *J. Geophys. Res.,* **103,** 12 649–12 668.

Thorpe, S. A., 1986: Measurements with an automatically recording inverted echo sounder: ARIES and the bubble clouds. *J. Phys. Oceanogr.,* **16,** 1462–1478.

Trump, C. L., N. Allan, and G. O. Marmorino, 1999: Using side-looking acoustic Doppler current profiler (ADCP) and Doppler radar systems to characterize a convergent surface front. *Proc. IEEE Sixth Working Conf. on Current Measurement,* San Diego, CA, IEEE, 131–135.

Vesecky, J. F., C. C. Teague, J. D. Paduan, D. M. Fernandez, K. Laws, Z. Hallock, and L. A. Meadows, 1998: Observations of air–sea dynamics by multifrequency HF radar and other environmental sensors outside the mouth of the Chesapeake Bay during the COPE-3 experiment of October–November 1997. *Eos, Trans. Amer. Geophys. Union,* **79**(1), 169.

Zedel, L., G. B. Crawford, and L. Gordon, 1996: On the determination of wind direction using an upward looking acoustic Doppler current profiler. *J. Geophys. Res.,* **101,** 12 163–12 176.